In situ tuning of dynamical Coulomb blockade on Andreev bound states in hybrid nanowire devices

Shan Zhang,[1,*] Zhichuan Wang,[2,*] Dong Pan,[3,*] Zhaoyu Wang,[1] Zonglin Li,[1] Zitong Zhang,[1] Yichun Gao,[1] Zhan Cao,[4] Gu Zhang,[4] Lei Liu,[3] Lianjun Wen,[3] Ran Zhuo,[3] Dong E. Liu,[1,4,5] Ke He,[1,4,5] Runan Shang,[4,†] Jianhua Zhao,[3,‡] and Hao Zhang[1,4,5,§]

[1]*State Key Laboratory of Low Dimensional Quantum Physics, Department of Physics, Tsinghua University, Beijing 100084, China*
[2]*Beijing National Laboratory for Condensed Matter Physics, Institute of Physics, Chinese Academy of Sciences, Beijing 100190, China*
[3]*State Key Laboratory of Superlattices and Microstructures, Institute of Semiconductors, Chinese Academy of Sciences, P.O. Box 912, Beijing 100083, China*
[4]*Beijing Academy of Quantum Information Sciences, Beijing 100193, China*
[5]*Frontier Science Center for Quantum Information, Beijing 100084, China*

(Received 4 January 2023; revised 20 September 2023; accepted 28 November 2023; published 12 December 2023)

Electron interactions in quantum devices can exhibit intriguing phenomena. One example is assembling an electronic device in series with an on-chip resistor. The quantum laws of electricity of the device are modified at low energies and temperatures by dissipative interactions induced by the resistor, a phenomenon known as the dynamical Coulomb blockade (DCB). The DCB strength is usually nonadjustable in a fixed environment defined by the resistor. Here, we design an on-chip circuit for InAs-Al hybrid nanowires where the DCB strength can be gate-tuned *in situ*. InAs-Al nanowires could host Andreev or Majorana zero-energy states. This technique enables tracking the evolution of the same state while tuning the DCB strength from weak to strong. We observe the transition from a zero-bias conductance peak to split peaks for Andreev zero-energy states. Our technique opens the door to *in situ* tuning interaction strength on zero-energy states.

DOI: 10.1103/PhysRevB.108.235416

I. INTRODUCTION

Hybrid semiconductor-superconductor nanowires provide an excellent platform for the realization of various quantum electronic devices such as supercurrent transistors [1], Cooper pair splitters [2], gate-tunable qubits [3], Andreev quantum point contacts [4], and possible Majorana zero modes (MZMs) [5–7]. These devices can combine the pairing correlations from the superconductor with low-dimensional gate-tunable carrier densities from the semiconductor, thus attracting much interest in both fundamental and application-wise research perspectives. A fascinating prediction is the MZMs [8,9] which hold promise toward topological quantum computations. Though enormous experimental efforts have been made in the quest for MZM signatures [10–15], the major uncertainty comes from Andreev bound states (ABSs) [16] which can form in the same device and mimic MZMs [17–24]. Both MZMs and ABSs can lead to similar zero-bias peaks (ZBPs) in tunneling conductance spectroscopy. Therefore, one of the top priorities along this roadmap is finding an effective diagnostic tool to distinguish these two scenarios.

Interactions could stabilize MZMs and suppress ABS signals. The mechanism is that interaction-induced renormalization sharpens the transitions between different physics to different fixed points [25]. One example is by adding an on-chip resistor (a few kΩ) in series with the MZM device [26]. The resistor provides a dissipative electromagnetic environment. Small tunnel junctions embedded in this interactive environment can reveal a conductance dip near zero energy at low temperatures [27–41]. This "dissipative tunneling" is also dubbed the environmental Coulomb blockade or dynamical Coulomb blockade (DCB). Since "dissipation" in the hybrid nanowire literature usually refers to soft gaps [42,43], so to avoid confusion, in this paper we adopt the term "DCB" to describe this interaction effect. The DCB strength scales with the environmental impedance that is determined by the on-chip resistor. A larger resistor leads to a stronger suppression of the zero-bias conductance. The key idea of the proposal [26,44] is that increasing the DCB strength splits ABS-induced ZBPs by suppressing the conductance at zero bias. As for MZMs, the ZBP is mediated by symmetric resonant Andreev reflections [45–48]. The topological ZBP could survive the DCB suppression and stay at the quantized value of $2e^2/h$ as long as the DCB strength is below a threshold (environmental impedance less than the resistance quantum $h/2e^2$) [26].

In recent experiments [49,50], we have introduced DCB into hybrid InAs-Al nanowire devices where the ABS-induced ZBPs can be indeed suppressed, leading to split peaks. The circuit design is two-terminal where the nanowire and the resistor are connected in series. The drawback of this design is that the DCB strength is nonadjustable for a fixed barrier once the resistor has been fabricated. This makes it difficult to judge whether the measured split peaks originate from a zero-energy ABS (an effect of DCB) or just a finite-energy ABS, which

*These authors contributed equally to this work.
†shangrn@baqis.ac.cn
‡jhzhao@semi.ac.cn
§hzquantum@mail.tsinghua.edu.cn

can result in split peaks even without DCB. Moreover, the resistance of the resistor could only be estimated indirectly, introducing another error source. This possible error can also affect the accuracy of ZBP heights since the nanowire resistance is obtained by subtracting the resistor resistance from the total resistance of the two-terminal circuit. In this paper, we demonstrate a different circuit with a three-terminal design that solves these problems. The DCB strength can be *in situ* tuned using a gate voltage on the third terminal. This technique enables us to increase the DCB strength and track the evolution of the same zero-energy ABS, i.e., a ZBP gradually evolves to split peaks. The resistances of the resistor and the nanowire can also be accurately measured. Our technique can not only serve as a powerful knob in the future Majorana detection, but also can facilitate more interaction-related physics experiments, e.g., the realization of a Berezinskii-Kosterlitz-Thouless quantum phase transition or emulating two-channel Kondo physics [37].

II. EXPERIMENTAL RESULTS

Figure 1(a) shows the scanning electron micrograph (SEM) of device A. An InAs-Al wire is contacted by three Ti/Au electrodes (yellow). The middle electrode is connected in series with a thin resistive Cr/Au film (red, 10 nm/2 nm in thickness), serving as the on-chip resistor. The resistance of the film, $R \sim 11.7$ kΩ, can be directly measured using the three-terminal setup [see Fig. S1 in the Supplemental Material (SM) for details [51]]. Directly measuring R was not feasible in previous two-terminal designs, where the value of R can only be indirectly inferred [49,50]. The wire growth details can be found in Ref. [52]. Three side gates (yellow, Ti/Au, thickness 5 nm/70 nm) are used: TG tunes the barrier part; SG tunes the proximitized bulk; SW serves as a DCB switch. The middle electrode forms an ohmic contact with the nanowire through Ar plasma etching. In this way, the nanowire is separated into two quantum conductors which are connected by the middle electrode. So the two segments of the nanowire (the barrier region and the SW region) can be treated separately, avoiding uncontrolled nonlocal effects.

The basic idea is sketched in Figs. 1(b) and 1(c). A voltage V_{Bias} is applied to the first electrode. The current I is measured after passing through the InAs-Al wire, the second electrode, and the film (R). The differential conductance of the InAs-Al wire is calculated as $G = dI/dV$, where $V = V_{\mathrm{Bias}} - I \times R$. The remaining InAs segment is connected to the third electrode (terminal), which extends all the way to the bonding pad on the chip. The bonding pad is connected to a fridge line whose room-temperature end is floated. The large capacitance of the pad ($C \sim 10$ pF) can short-circuit the high-frequency quantum fluctuations. Since the DCB strength is determined by the environmental impedance regarding a frequency range from 0 to tens of GHz, the capacitor C can significantly reduce this high-frequency impedance if the InAs segment is opened by SW. In this way, even though the dc current solely flows through the InAs-Al wire and R, the third terminal (opened for dc but grounded for high frequency) can reduce the DCB effect induced by R. We call this regime the weak DCB. A zero-energy ABS, formed near the barrier, will be resolved as a ZBP at low (but finite) temperatures. If 0 K could be reached,

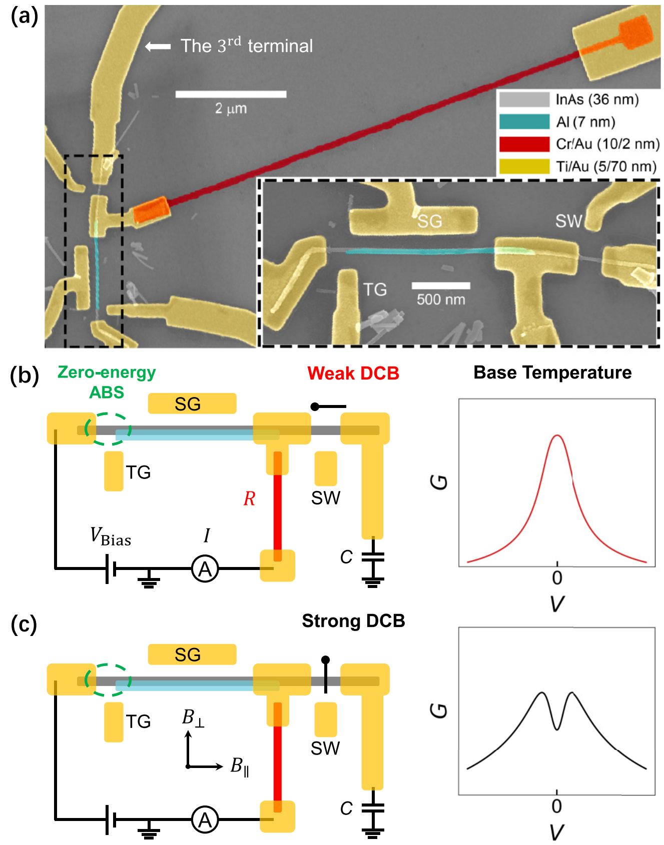

FIG. 1. (a) SEM of device A (false colored). Inset: Zoom-in of the InAs-Al part. The substrate is *p*-doped Si covered by 300-nm-thick SiO_2. The Si (back gate) was grounded throughout the measurement. (b) Left: A simplified schematic of the circuit diagram. The switch (SW) gate turns on the InAs segment nearby, shunting the dissipative resistor (weak DCB). Right: A zero-energy ABS resolves a ZBP (not in scale) at a finite fridge temperature. (c) Left: SW pinches off the InAs segment (strong DCB). Right: The same zero-energy ABS resolves split peaks due to the suppression of G at zero bias.

regardless of how weak is the DCB strength, the zero-bias tunneling G could always be suppressed to zero, splitting the ABS-induced ZBPs. More negative gate voltage on SW can pinch off the InAs segment and restore the DCB induced by R [Fig. 1(c)]. In this strong DCB regime, an ABS-induced ZBP will split due to the strong suppression of G at zero bias. The right panels sketch the conductance line shapes (not in scale) in the two cases. We note that similar ideas of tuning DCB using a gate switch and large capacitors, i.e., the three-terminal geometry, have been previous implemented in the system of two-dimensional electron gases [32,33,38].

In Fig. 2, we characterize the DCB strength in device A. A perpendicular magnetic field of 1 T [see Fig. 1(c) for the B orientation] drives the device normal. DCB effects in a normal tunnel junction have been well studied [27–30]. Figures 2(a) and 2(b) show the characteristic suppression near zero bias and the T dependence at $V_{\mathrm{SW}} = 10$ V (segment fully opened, weak DCB) and −20 V (segment pinched off, strong DCB). For the V_{SW} dependence of the segment conductance, see Fig. S1 in SM [51]. The suppression of zero-bias G (at

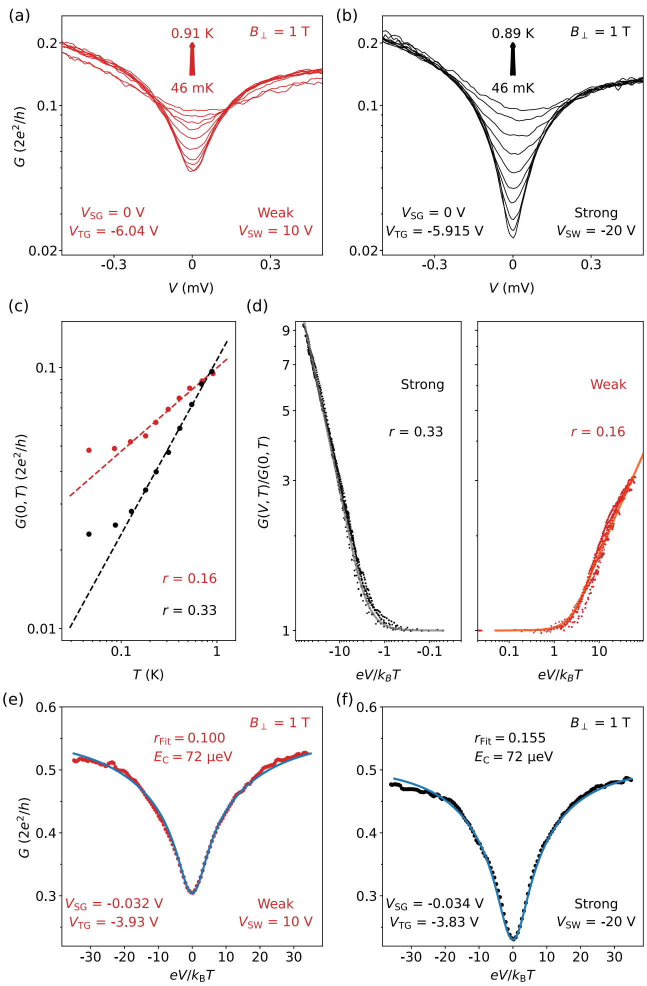

FIG. 2. (a) Zero-bias suppression of the normal state G ($B_\perp = 1$ T) in the weak DCB regime ($V_{SW} = 10$ V). $V_{TG} = -6.04$ V, $V_{SG} = 0$ V. The fridge T varies from 46 mK to 0.91 K for different curves. (b) T dependence in the strong DCB regime ($V_{SW} = -20$ V) at a similar barrier transmission. $V_{TG} = -5.915$ V, $V_{SG} = 0$ V. (c) T dependence of the zero-bias G, extracted from (a) (red) and (b) (black). Dashed lines are the power-law fits with the exponents (r) labeled. (d) Replotting all the curves in (a) (right) and (b) (left) using dimensionless units. The solid lines are fits using the extracted r's from (c). (e) The DCB dip at base T in the weak DCB regime with a higher barrier transmission. The blue solid line is the fit using the $P(E)$ theory. The effective temperature is assumed to be ~100 mK. The charging energy is extracted to be 72 μeV. (f) Similar to (e) but in the strong DCB regime.

base T) in the weak DCB regime is indeed weaker than the strong DCB case. Note that the y axis is in the logarithmic scale to highlight this difference. The tunnel transmissions for Figs. 2(a) and 2(b) are similar, reflected by the G's at high T (0.9 K). Keeping the same transmission is important for this comparison since the DCB strength can also be modified by the barrier transparency and scales with the Fano factor [32,33,41].

A more quantitative description of the "zero-bias dip" is the power law: $G \propto \max(k_BT, eV)^{2r}$ [29]. The exponent r determines the effective environmental impedance ($r \times h/e^2$) and the DCB strength. Figure 2(c) shows the extracted zero-bias G's from Figs. 2(a) and 2(b). The dashed lines are the temperature power-law fits ($G \propto T^{2r}$), revealing r of 0.16 for the weak and 0.33 for the strong DCB cases. The deviations below 100 mK suggest a gradual saturation of the device electron T.

Figure 2(d) plots all the curves in Figs. 2(a) and 2(b) (over half of the bias branch) using dimensionless units: $G(V,T)/G(0,T)$ for the y axis and eV/k_BT for the x axis. All curves "collapse" onto a single universal line with minor deviations (the gray line for the strong and the red for the weak DCB regimes). The "linear trend" in this log-log plot for the regions of $|eV/k_BT| > 1$ suggests the power law for V. The universal line is a prediction of the conventional DCB theory and obtained by performing numerical differentiation on the formula [34] $I(V,T) \propto VT^{2r}|\Gamma(r+1+ieV/2\pi k_BT)/\Gamma(1+ieV/2\pi k_BT)|^2$, where Γ is the gamma function. r is extracted from Fig. 2(c). For $T < 100$ mK, we used the electron T [extracted from Fig. 2(c)] for the x axis in Fig. 2(d). For more power-law analysis and its SW tunability, see Fig. S2 for device A, Fig. S3 for device B, and Fig. S4 for device C in SM [51].

The power law holds over only a half order of magnitude [Fig. 2(c)], due to a relatively small dissipative resistor R. In our previous work [49] where R is much larger, the power-law range can exceed an order of magnitude. Since a power law over a short range has a limited implication, to better characterize the DCB dip we have performed the $P(E)$ calculation [29,38,53]. $P(E)$ theory can capture the conductance features at higher energies (outside the cutoff energy where the power law no longer holds). Figures 2(e) and 2(f) show the $P(E)$ fitting (blue curves) in the weak and strong DCB regimes, agreeing reasonable well with the experiment. The input parameters are the charging energy of the tunnel junction ($E_C = 72$ μeV), the effective T (~100 mK), and r as the fitting parameter (see SM for the calculation details). The fitted r (r_{Fit}) is indeed smaller in the weak DCB regime than that in the strong DCB regime.

After establishing the *in situ* tunability of DCB strength in the normal state regime, we now study ABSs in the superconducting regime by aligning B parallel to the nanowire axis (device A). In Fig. 3(a), a finite-energy ABS at zero field moves to zero energy at $B \sim 0.7$ T. In the weak DCB regime (upper), this process reveals a level crossing and a ZBP at 0.7 T [Fig. 3(b)]. In the strong DCB regime (lower), the crossing becomes anticrossing and the ZBP splits at 0.7 T. This peak splitting does not originate from a finite-energy ABS but reflects the DCB effect on a zero-energy ABS. We can confirm this by tracing the same state back to the weak DCB regime. The small differences of V_{TG} (and V_{SG}) between the weak and strong DCB regimes are to compensate for the residue crosstalk with SW, ensuring that the same ABS is being monitored during the DCB tuning.

The transition from "level-crossing ZBP" in the weak DCB regime to "anticrossing split peaks" in the strong DCB regime for the same ABS is enabled by our technique: the three-terminal circuit design (the main advancement of this work). This transition can also be revealed in the gate scans of the same ABS [see Figs. 3(c) and 3(d)]. The overall G of the ABS in Fig. 3, $\sim e^2/h$, is significantly higher than that in Fig. 2, suggesting a higher barrier transparency. Higher trans-

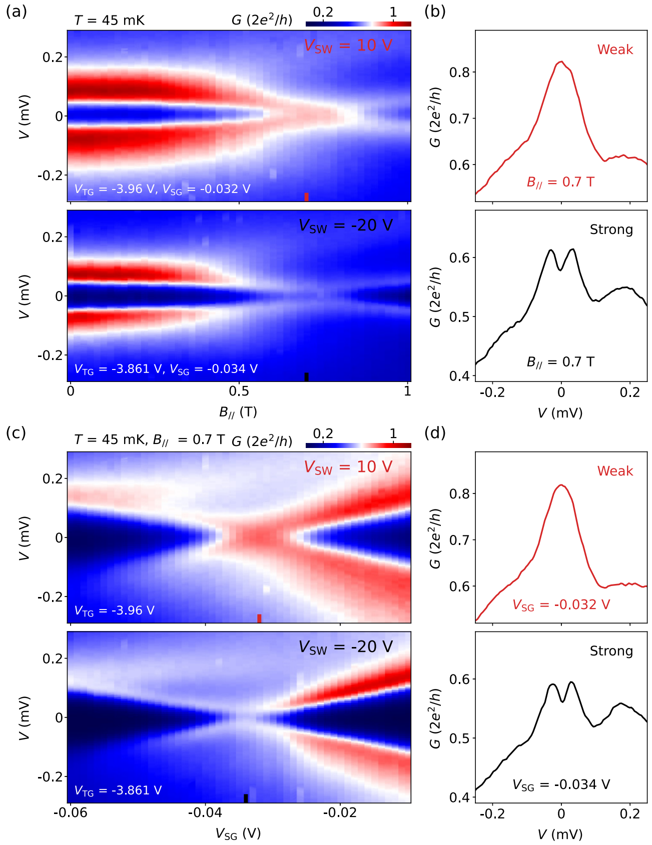

FIG. 3. (a) B dependence of an ABS in the weak (upper, $V_{\mathrm{SW}} = 10$ V) and strong (lower, $V_{\mathrm{SW}} = -20$ V) DCB regimes. (b) Line cuts at $B = 0.7$ T. (c) Gate dependence of this ABS at 0.7 T in the weak (upper) and strong (lower) DCB regimes. (d) Line cuts of (c) at the "crossing points."

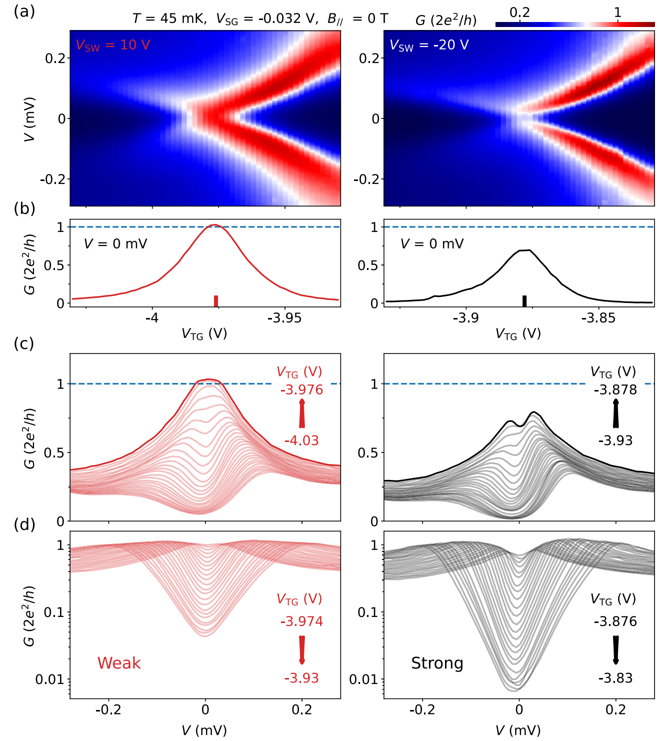

FIG. 4. (a) Gate dependence of a ZBP whose height is fine-tuned to $2e^2/h$ in the weak (left) and strong (right) DCB regimes. (b) Zero-bias line cuts from (a). (c) Waterfall plots for the left half of the gate ranges in (a). The top curves correspond the gate voltages indicated by the bars in (b). (d) Waterfall plots for the other half of the gate range. The y axis is in logarithmic scale.

parency can "weaken" the DCB effect [32,33,41] [see also Figs. 2(a) and 2(b) versus Figs. 2(e) and 2(f)]. To verify the validity of our technique in this high transparency regime, in Fig. S5 in SM [51] we show the power law of the normal state G and the SW-tunable r at $G \sim e^2/h$. Note that the suppression of conductance in the normal state and superconducting (ABS) regime may differ. In the normal state, $G \propto T^{2r}$, while for ABS, $G \propto T^{4r}$ or T^{8r} due to Andreev reflections. The exponents of $8r$ and $4r$ originate from the coherent and incoherent Andreev reflections, respectively [44]. Other values of exponents are also possible when different processes mix together. Nevertheless, the tunable r (by SW) combined with the qualitative change from ZBP to split peaks constitute a powerful tool to *in situ* identify ABSs. Figure S6 in SM [51] shows additional scans for intermediate V_{SW}, ranging from 10 and −20 V, as well as V_{TG} scans.

Whether or not tuning the DCB strength could split an ABS-induced ZBP depends on many factors, e.g., the device temperature, the details of the ABS, and to what extent r can be tuned or varied. Figures S7 and S8 in SM [51] show results from device B where the tunable range of r is smaller: from ∼0.05 to 0.13. As a result, the suppression (splitting) of ABS-induced ZBPs is less effective: Only parts of the ZBP regions in the parameter space show the splitting by increasing r (Fig. S7). Figure S8 monitors the continuous change of a finite-energy ABS.

The ZBPs so far are smaller than $2e^2/h$, obviously not MZMs but ABS induced. A natural follow-up question is as follows: How will $2e^2/h$ ZBPs evolve by varying the DCB strength? A previous theoretical work [26] predicts that the height of MZM-induced ZBPs will not be affected for $r < 0.5$ and will robustly stick to the quantized value. While ZBPs forming $2e^2/h$ plateaus are rare [15], finding them and testing their stability by tuning r are the goal of our future study. In Fig. 4 we address a related question by studying a ZBP fine-tuned to $2e^2/h$.

Figure 4(a) (the left panel) shows the gate dependence of this ABS in device A. MZMs are not expected since $B = 0$ T. The ZBP height is accidentally close to $2e^2/h$. This $2e^2/h$ peak is fine-tuned since the zero-bias G does not resolve a plateau [Fig. 4(b), the red curve]. Increasing the DCB strength from weak to strong, the zero-bias G gets significantly suppressed [Fig. 4(b), the black curve]. In addition, the ZBP in the weak DCB regime becomes split peaks in the strong DCB regime [see the top red and black line cuts in Fig. 4(c) and the color maps in Fig. 4(a)]. The zero-bias G of split peaks in the weak DCB regime, corresponding finite-energy ABSs, is also suppressed when tuned into the strong DCB regime. In Fig. 4(c) we show this suppression in linear scale to highlight the high G part. The V_{TG} ranges correspond to the left sides of the bars in Fig. 4(b). In Fig. 4(d), logarithmic scale is used to highlight the difference in the lower G regimes. The V_{TG} ranges correspond to the right sides of the bars in Fig. 4(b). For the V_{SG} dependence of this ABS, see Fig. S9 in SM [51].

ZBPs fine-tuned to $2e^2/h$ have recently raised intense discussion on possible false-positive signatures of MZMs [24]. Figure 4 shows that these peaks could be identified and safely "filtered out" by our technique in the search of true quantized peaks.

III. CONCLUSION

To summarize, we have established a three-terminal circuit technique which enables the *in situ* tuning of the DCB strength in hybrid semiconductor-superconductor nanowire devices. This technique allows us to "diagnose" the origins of zero-energy states by changing the interaction strength. Zero-bias peaks induced by Andreev bound states with heights at nonquantized values or accidentally at $2e^2/h$ can be split (filtered out) by increasing the DCB strength. The tunability of the DCB strength is determined by the SW segment of the nanowire. Using a second (thick) nanowire as the SW segment could improve this tunability. By tuning the interaction *in situ*, our result paves the way toward finding cleaner and stronger evidence of Majorana zero modes in future studies.

Raw data and processing codes within this paper are available [54].

ACKNOWLEDGMENTS

This work is supported by Tsinghua University Initiative Scientific Research Program, National Natural Science Foundation of China (Grants No. 12104053, No. 92065106, No. 92065206, No. 61974138, No. 12004040, No. 11974198, and No. 12374158). D.P. also acknowledges the support from Youth Innovation Promotion Association, Chinese Academy of Sciences (Grants No. 2017156 and No. Y2021043).

[1] Y.-J. Doh, J. A. van Dam, A. L. Roest, E. P. A. M. Bakkers, L. P. Kouwenhoven, and S. D. Franceschi, Tunable supercurrent through semiconductor nanowires, Science **309**, 272 (2005).

[2] L. Hofstetter, S. Csonka, J. Nygård, and C. Schoenenberger, Cooper pair splitter realized in a two-quantum-dot Y-junction, Nature (London) **461**, 960 (2009).

[3] T. W. Larsen, K. D. Petersson, F. Kuemmeth, T. S. Jespersen, P. Krogstrup, J. Nygård, and C. M. Marcus, Semiconductor-nanowire-based superconducting qubit, Phys. Rev. Lett. **115**, 127001 (2015).

[4] H. Zhang, Ö. Gül, S. Conesa-Boj, M. P. Nowak, M. Wimmer, K. Zuo, V. Mourik, F. K. De Vries, J. Van Veen, M. W. De Moor *et al.*, Ballistic superconductivity in semiconductor nanowires, Nat. Commun. **8**, 16025 (2017).

[5] E. Prada, P. San-Jose, M. W. de Moor, A. Geresdi, E. J. Lee, J. Klinovaja, D. Loss, J. Nygård, R. Aguado, and L. P. Kouwenhoven, From Andreev to Majorana bound states in hybrid superconductor–semiconductor nanowires, Nat. Rev. Phys. **2**, 575 (2020).

[6] H. Zhang, D. E. Liu, M. Wimmer, and L. P. Kouwenhoven, Next steps of quantum transport in Majorana nanowire devices, Nat. Commun. **10**, 5128 (2019).

[7] P. Marra, Majorana nanowires for topological quantum computation, J. Appl. Phys. **132**, 231101 (2022).

[8] R. M. Lutchyn, J. D. Sau, and S. Das Sarma, Majorana fermions and a topological phase transition in semiconductor-superconductor heterostructures, Phys. Rev. Lett. **105**, 077001 (2010).

[9] Y. Oreg, G. Refael, and F. von Oppen, Helical liquids and Majorana bound states in quantum wires, Phys. Rev. Lett. **105**, 177002 (2010).

[10] V. Mourik, K. Zuo, S. M. Frolov, S. Plissard, E. P. Bakkers, and L. P. Kouwenhoven, Signatures of Majorana fermions in hybrid superconductor-semiconductor nanowire devices, Science **336**, 1003 (2012).

[11] M. Deng, S. Vaitiekėnas, E. B. Hansen, J. Danon, M. Leijnse, K. Flensberg, J. Nygård, P. Krogstrup, and C. M. Marcus, Majorana bound state in a coupled quantum-dot hybrid-nanowire system, Science **354**, 1557 (2016).

[12] Ö. Gül, H. Zhang, J. D. Bommer, M. W. de Moor, D. Car, S. R. Plissard, E. P. Bakkers, A. Geresdi, K. Watanabe, T. Taniguchi *et al.*, Ballistic Majorana nanowire devices, Nat. Nanotechnol. **13**, 192 (2018).

[13] H. Zhang, M. W. de Moor, J. D. Bommer, D. Xu, G. Wang, N. van Loo, C.-X. Liu, S. Gazibegovic, J. A. Logan, D. Car *et al.*, Large zero-bias peaks in InSb-Al hybrid semiconductor-superconductor nanowire devices, arXiv:2101.11456.

[14] H. Song, Z. Zhang, D. Pan, D. Liu, Z. Wang, Z. Cao, L. Liu, L. Wen, D. Liao, R. Zhuo, D. E. Liu, R. Shang, J. Zhao, and H. Zhang, Large zero bias peaks and dips in a four-terminal thin InAs-Al nanowire device, Phys. Rev. Res. **4**, 033235 (2022).

[15] Z. Wang, H. Song, D. Pan, Z. Zhang, W. Miao, R. Li, Z. Cao, G. Zhang, L. Liu, L. Wen, R. Zhuo, D. E. Liu, K. He, R. Shang, J. Zhao, and H. Zhang, Plateau regions for zero-bias peaks within 5% of the quantized conductance value $2e^2/h$, Phys. Rev. Lett. **129**, 167702 (2022).

[16] A. Andreev, Electron spectrum of the intermediate state of superconductors, Sov. Phys. JETP **22**, 18 (1966).

[17] E. Prada, P. San-Jose, and R. Aguado, Transport spectroscopy of NS nanowire junctions with Majorana fermions, Phys. Rev. B **86**, 180503(R) (2012).

[18] G. Kells, D. Meidan, and P. W. Brouwer, Near-zero-energy end states in topologically trivial spin-orbit coupled superconducting nanowires with a smooth confinement, Phys. Rev. B **86**, 100503(R) (2012).

[19] E. J. Lee, X. Jiang, M. Houzet, R. Aguado, C. M. Lieber, and S. De Franceschi, Spin-resolved Andreev levels and parity crossings in hybrid superconductor–semiconductor nanostructures, Nat. Nanotechnol. **9**, 79 (2014).

[20] C.-X. Liu, J. D. Sau, T. D. Stanescu, and S. Das Sarma, Andreev bound states versus Majorana bound states in quantum dot-nanowire-superconductor hybrid structures: Trivial versus topological zero-bias conductance peaks, Phys. Rev. B **96**, 075161 (2017).

[21] C. Reeg, O. Dmytruk, D. Chevallier, D. Loss, and J. Klinovaja, Zero-energy Andreev bound states from quantum dots in proximitized Rashba nanowires, Phys. Rev. B **98**, 245407 (2018).

[22] C. Moore, C. Zeng, T. D. Stanescu, and S. Tewari, Quantized zero-bias conductance plateau in semiconductor-superconductor heterostructures without topological Majorana zero modes, Phys. Rev. B **98**, 155314 (2018).

[23] A. Vuik, B. Nijholt, A. Akhmerov, and M. Wimmer, Reproducing topological properties with quasi-Majorana states, SciPost Phys. **7**, 061 (2019).

[24] H. Pan and S. Das Sarma, Physical mechanisms for zero-bias conductance peaks in Majorana nanowires, Phys. Rev. Res. **2**, 013377 (2020).

[25] J. Cardy, *Scaling and Renormalization in Statistical Physics*, Cambridge Lecture Notes in Physics (Cambridge University Press, Cambridge, UK, 1996).

[26] D. E. Liu, Proposed method for tunneling spectroscopy with ohmic dissipation using resistive electrodes: A possible Majorana filter, Phys. Rev. Lett. **111**, 207003 (2013).

[27] P. Delsing, K. K. Likharev, L. S. Kuzmin, and T. Claeson, Effect of high-frequency electrodynamic environment on the single-electron tunneling in ultrasmall junctions, Phys. Rev. Lett. **63**, 1180 (1989).

[28] M. H. Devoret, D. Esteve, H. Grabert, G.-L. Ingold, H. Pothier, and C. Urbina, Effect of the electromagnetic environment on the Coulomb blockade in ultrasmall tunnel junctions, Phys. Rev. Lett. **64**, 1824 (1990).

[29] G. L. Ingold and Y. V. Nazarov, in *Single Charge Tunnelling: Coulomb Blockade Phenomena in Nanostructures*, edited by H. Grabert and M. H. Devoret (Springer, New York, 1992), pp. 21–107.

[30] K. Flensberg, S. M. Girvin, M. Jonson, D. R. Penn, and M. D. Stiles, Quantum mechanics of the electromagnetic environment in the single-junction coulomb blockade, Phys. Scr., **T42**, 189 (1992).

[31] F. Pierre, H. Pothier, P. Joyez, N. O. Birge, D. Esteve, and M. H. Devoret, Electrodynamic dip in the local density of states of a metallic wire, Phys. Rev. Lett. **86**, 1590 (2001).

[32] C. Altimiras, U. Gennser, A. Cavanna, D. Mailly, and F. Pierre, Experimental test of the dynamical Coulomb blockade theory for short coherent conductors, Phys. Rev. Lett. **99**, 256805 (2007).

[33] F. Parmentier, A. Anthore, S. Jezouin, H. Le Sueur, U. Gennser, A. Cavanna, D. Mailly, and F. Pierre, Strong back-action of a linear circuit on a single electronic quantum channel, Nat. Phys. **7**, 935 (2011).

[34] H. T. Mebrahtu, I. V. Borzenets, D. E. Liu, H. Zheng, Y. V. Bomze, A. I. Smirnov, H. U. Baranger, and G. Finkelstein, Quantum phase transition in a resonant level coupled to interacting leads, Nature (London) **488**, 61 (2012).

[35] H. Mebrahtu, I. Borzenets, H. Zheng, Y. V. Bomze, A. Smirnov, S. Florens, H. Baranger, and G. Finkelstein, Observation of Majorana quantum critical behaviour in a resonant level coupled to a dissipative environment, Nat. Phys. **9**, 732 (2013).

[36] L. Serrier-Garcia, J. C. Cuevas, T. Cren, C. Brun, V. Cherkez, F. Debontridder, D. Fokin, F. S. Bergeret, and D. Roditchev, Scanning tunneling spectroscopy study of the proximity effect in a disordered two-dimensional metal, Phys. Rev. Lett. **110**, 157003 (2013).

[37] D. E. Liu, H. Zheng, G. Finkelstein, and H. U. Baranger, Tunable quantum phase transitions in a resonant level coupled to two dissipative baths, Phys. Rev. B **89**, 085116 (2014).

[38] S. Jezouin, M. Albert, F. Parmentier, A. Anthore, U. Gennser, A. Cavanna, I. Safi, and F. Pierre, Tomonaga–Luttinger physics in electronic quantum circuits, Nat. Commun. **4**, 1802 (2013).

[39] A. Anthore, Z. Iftikhar, E. Boulat, F. D. Parmentier, A. Cavanna, A. Ouerghi, U. Gennser, and F. Pierre, Circuit quantum simulation of a Tomonaga-Luttinger liquid with an impurity, Phys. Rev. X **8**, 031075 (2018).

[40] K. Wölms and K. Flensberg, Environmental Coulomb blockade of topological superconductor-normal metal junctions, Phys. Rev. B **92**, 165428 (2015).

[41] J. Senkpiel, J. C. Klöckner, M. Etzkorn, S. Dambach, B. Kubala, W. Belzig, A. L. Yeyati, J. C. Cuevas, F. Pauly, J. Ankerhold, C. R. Ast, and K. Kern, Dynamical Coulomb blockade as a local probe for quantum transport, Phys. Rev. Lett. **124**, 156803 (2020).

[42] S. Takei, B. M. Fregoso, H.-Y. Hui, A. M. Lobos, and S. Das Sarma, Soft superconducting gap in semiconductor Majorana nanowires, Phys. Rev. Lett. **110**, 186803 (2013).

[43] C.-X. Liu, J. D. Sau, and S. Das Sarma, Role of dissipation in realistic Majorana nanowires, Phys. Rev. B **95**, 054502 (2017).

[44] D. Liu, G. Zhang, Z. Cao, H. Zhang, and D. E. Liu, Universal conductance scaling of Andreev reflections using a dissipative probe, Phys. Rev. Lett. **128**, 076802 (2022).

[45] K. Sengupta, I. Žutić, H.-J. Kwon, V. M. Yakovenko, and S. Das Sarma, Midgap edge states and pairing symmetry of quasi-one-dimensional organic superconductors, Phys. Rev. B **63**, 144531 (2001).

[46] K. T. Law, P. A. Lee, and T. K. Ng, Majorana fermion induced resonant Andreev reflection, Phys. Rev. Lett. **103**, 237001 (2009).

[47] K. Flensberg, Tunneling characteristics of a chain of Majorana bound states, Phys. Rev. B **82**, 180516(R) (2010).

[48] Y. Asano and Y. Tanaka, Majorana fermions and odd-frequency Cooper pairs in a normal-metal nanowire proximity-coupled to a topological superconductor, Phys. Rev. B **87**, 104513 (2013).

[49] S. Zhang, Z. Wang, D. Pan, H. Li, S. Lu, Z. Li, G. Zhang, D. Liu, Z. Cao, L. Liu, L. Wen, D. Liao, R. Zhuo, R. Shang, D. E. Liu, J. Zhao, and H. Zhang, Suppressing Andreev bound state zero bias peaks using a strongly dissipative lead, Phys. Rev. Lett. **128**, 076803 (2022).

[50] Z. Wang, S. Zhang, D. Pan, G. Zhang, Z. Xia, Z. Li, D. Liu, Z. Cao, L. Liu, L. Wen, D. Liao, R. Zhuo, Y. Li, D. E. Liu, R. Shang, J. Zhao, and H. Zhang, Large Andreev bound state zero-bias peaks in a weakly dissipative environment, Phys. Rev. B **106**, 205421 (2022).

[51] See Supplemental Material at http://link.aps.org/supplemental/10.1103/PhysRevB.108.235416 for additional data and analysis.

[52] D. Pan, H. Song, S. Zhang, L. Liu, L. Wen, D. Liao, R. Zhuo, Z. Wang, Z. Zhang, S. Yang, J. Ying, W. Miao, R. Shang, H. Zhang, and J. Zhao, *In situ* epitaxy of pure phase ultra-thin InAs-Al nanowires for quantum devices, Chin. Phys. Lett. **39**, 058101 (2022).

[53] K. Flensberg and M. Jonson, Quantum fluctuations and charging effects in small tunnel junctions, Phys. Rev. B **43**, 7586 (1991).

[54] https://doi.org/10.5281/zenodo.7317835.